Escape fractions from unattenuated Lyα emitters around luminous z > 6 quasars

Yue, M.; Eilers, A.-C.; Matthee, J.; Naidu, R.P.; Bordoloi, R.; Davies, F.B.; ... ; Simcoe, R.A.

Citation

Escape Fractions from Unattenuated Lyα Emitters around Luminous $z > 6$ Quasars

Minghao Yue[1,2] , Anna-Christina Eilers[1] , Jorryt Matthee[3] , Rohan P. Naidu[1,10] , Rongmon Bordoloi[4] ,
Frederick B. Davies[5] , Joseph F. Hennawi[6,7] , Daichi Kashino[8] , Ruari Mackenzie[9] , and Robert A. Simcoe[1]

[1] MIT Kavli Institute for Astrophysics and Space Research, 77 Massachusetts Ave., Cambridge, MA 02139, USA; myue@mit.edu
[2] Steward Observatory, University of Arizona, 933 N. Cherry Ave., Tucson, AZ 85721, USA
[3] Institute of Science and Technology Austria (ISTA), Am Campus 1, 3400 Klosterneuburg, Austria
[4] Department of Physics, North Carolina State University, Raleigh, NC 27695, USA
[5] Max Planck Institut für Astronomie, Königstuhl 17, D-69117 Heidelberg, Germany
[6] Department of Physics, University of California, Santa Barbara, CA 93106-9530, USA
[7] Leiden Observatory, Leiden University, PO Box 9513, 2300 RA Leiden, The Netherlands
[8] National Astronomical Observatory of Japan, 2-21-1 Osawa, Mitaka, Tokyo 181-8588, Japan
[9] Institute of Physics, Laboratory of Astrophysics, Ecole Polytechnique Fédérale de Lausanne (EPFL), and Observatoire de Sauverny, 1290 Versoix, Switzerland
Received 2025 July 5; revised 2025 September 5; accepted 2025 September 21; published 2025 October 24

Abstract

Ionized proximity zones around luminous quasars provide a unique laboratory to characterize the Lyα emission lines from $z > 6$ galaxies without significant attenuation from the intergalactic medium (IGM). However, Lyα line measurements for galaxies within high-redshift quasars' proximity zones have been rare so far. Here we present deep spectroscopic observations obtained with the NIRSpec/Micro-Shutter Assembly (MSA) instrument on the James Webb Space Telescope of galaxies in two $z > 6$ quasar fields. We measure the Lyα line fluxes for 50 galaxies at $6 < z < 7$ with UV absolute magnitude $M_{\rm UV} < -19$ (median $M_{\rm UV} = -19.97$), among which 15 are located near the luminous quasars, i.e., within $\Delta v < 2500 \, \rm km \, s^{-1}$. We find that galaxies near the quasars show significant flux blueward of the systemic Lyα wavelength, and have higher Lyα equivalent width compared to galaxies at similar redshifts that are not located within the quasars' environment. Our result indicates little or no redshift evolution for the Lyα emitter fraction from $z \sim 6.4$ to $z \sim 5$. Leveraging the low IGM opacity in the quasars' vicinity, we evaluate the Lyα escape fraction ($f_{\rm esc}^{\rm Ly\alpha}$) of high-redshift galaxies. Our analysis suggests that galaxies at $\langle z \rangle \approx 6.4$ have an average $f_{\rm esc}^{\rm Ly\alpha} = 0.14 \pm 0.04$. This value is consistent with reionization models where the Lyman continuum escape fraction is low ($f_{\rm esc}^{\rm LyC} \lesssim 0.1$) for luminous galaxies, and where the most luminous galaxies have only a minor contribution to the total ionizing photon budget.

Unified Astronomy Thesaurus concepts: High-redshift galaxies (734); Quasars (1319); Reionization (1383)

Materials only available in the online version of record: machine-readable table

1. Introduction

The Epoch of Reionization (EoR) represents the last major phase transition of the Universe, where the neutral hydrogen fraction of the intergalactic medium (IGM) changes from ~ 1 to ~ 0 between redshift $z \sim 20$ and $z \sim 5.5$ (e.g., S. E. I. Bosman et al. 2022; B. E. Robertson 2022). The overall history of reionization has been constrained by various observations, including the cosmic microwave background measurements (e.g., Planck Collaboration et al. 2020), quasar transmission fluxes and damping wings (e.g., X. Fan et al. 2006; J. Yang et al. 2020; X. Jin et al. 2023; D. Ďurovčíková et al. 2024), and Lyα lines from high-redshift galaxies (e.g., C. A. Mason et al. 2018, 2019; I. G. B. Wold et al. 2022; M. Tang et al. 2024a; Y. Kageura et al. 2025; H. Umeda et al. 2025). Nonetheless, it is still under debate which type of source dominates the ionizing photon production. Specifically, several studies have suggested that luminous galaxies make a major contribution to reionization (e.g., M. Sharma et al. 2016; R. P. Naidu et al. 2020; J. Matthee et al. 2022), while others found that the ionizing photon production is dominated by faint galaxies (e.g., R. J. Bouwens et al. 2012; S. L. Finkelstein et al. 2019; H. Atek et al. 2024).

One reason for this debate is the highly uncertain Lyman continuum (LyC) escape fraction ($f_{\rm esc}^{\rm LyC}$) for the EoR galaxies. Due to the high IGM opacity to LyC photons at $z \gtrsim 6$, it is impossible to directly measure the leaking LyC flux from EoR galaxies. Several indirect methods have been employed to infer the escape fraction of galaxies at $z \gtrsim 6$, including observations for low-redshift counterparts of $z > 6$ galaxies (e.g., Y. I. Izotov et al. 2018; R. P. Naidu et al. 2018; C. C. Steidel et al. 2018), computing the ionizing photon budget that is needed to produce the observed neutral fraction evolution (e.g., S. L. Finkelstein et al. 2019; R. P. Naidu et al. 2020; B. E. Robertson 2022), and adopting predictions from cosmological simulations (e.g., X. Ma et al. 2015, 2016; J. Rosdahl et al. 2022). Nevertheless, the inferred LyC escape fraction shows large discrepancies, ranging from $f_{\rm esc}^{\rm LyC} \lesssim 5\%$ (e.g., J. Chisholm et al. 2022; S. Mascia et al. 2023; C. Simmonds et al. 2024; C. Papovich et al. 2025) to $f_{\rm esc}^{\rm LyC} \gtrsim 20\%$ (e.g., R. P. Naidu et al. 2020; A. E. Jaskot et al. 2024).

At $4 \lesssim z \lesssim 5$, where the IGM is mostly opaque to LyC photons but has high transmission to Lyα lines from galaxies (e.g., R. A. Meyer et al. 2025), the LyC escape fraction of galaxies can be estimated using the escape fraction of the Lyα emission line ($f_{\rm esc}^{\rm Ly\alpha}$; e.g., Y. I. Izotov et al. 2022; R. Begley et al. 2024). However, this method is not applicable to most galaxies in the EoR, as the Lyα line is heavily attenuated by the neutral

---

[10] NHFP Hubble Fellow.
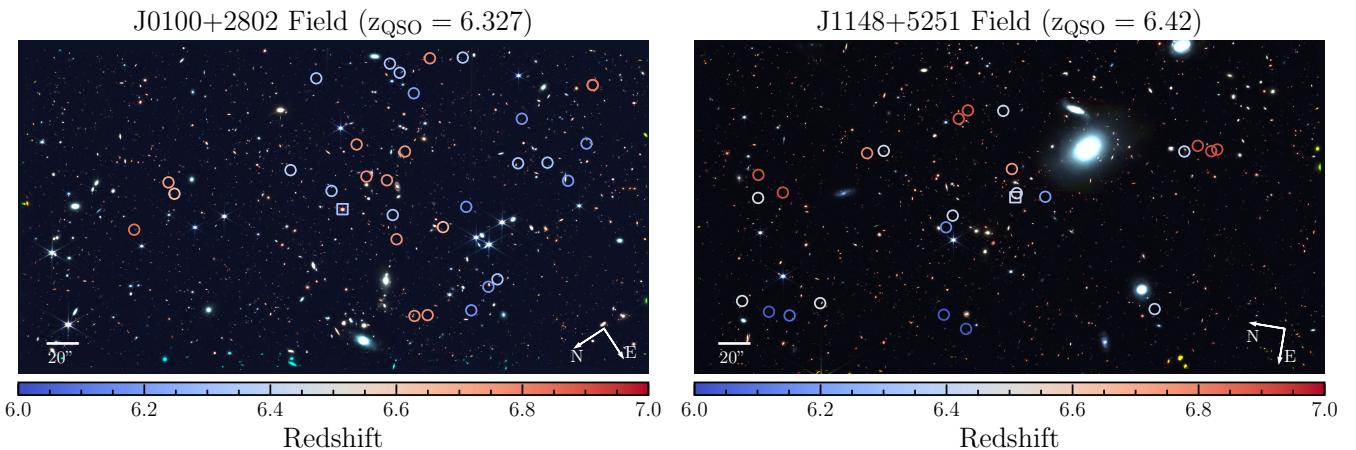
Figure 1. The two quasar fields targeted by this work, J0100+2802 (left) and J1148+5251 (right). We compose the red, green, and blue images using the NIRCam F115W, F200W, and F356W images from the EIGER project (e.g., D. Kashino et al. 2023). The quasars are at the field centers, marked by the squares. The circles mark the galaxy sample of this study, with the colors representing their systemic redshifts. There are 28 targets and 22 targets in the J0100+2802 and J1148+5251 fields, respectively.

hydrogen in the $z > 6$ IGM. The only viable approach to measure the unattenuated Lyα lines from EoR galaxies is to target galaxies that reside in ionized bubbles, where the IGM is transparent to Lyα photons (e.g., J. Matthee et al. 2018; A. Torralba et al. 2024; L. Whitler et al. 2024; Z. Chen et al. 2025; T.-Y. Lu et al. 2025). Such ionized bubbles are often produced by galaxy overdensities, and finding these ionized bubbles requires deep spectroscopy over wide fields (e.g., I. Nikolić et al. 2025).

In this context, proximity zones of high-redshift quasars offer a unique opportunity to investigate the unattenuated Lyα properties of EoR galaxies (e.g., S. E. I. Bosman et al. 2020; K. Protušová et al. 2024). Quasars at $z > 6$ are expected to produce large ionized bubbles around them, as implied by radiative transfer simulations (e.g., F. B. Davies 2020). Deep spectroscopy for galaxies residing in the proximity of high-redshift quasars will put direct constraints on the Lyα line properties of these galaxies.

In this work, we present James Webb Space Telescope (JWST) NIRSpec/MSA spectroscopy for galaxies near two $z > 6$ quasars, i.e., J0100+2802 ($z = 6.327$) and J1148+5251 ($z = 6.42$). We analyze the Lyα line properties of these galaxies, and try to answer the following questions. (1) For galaxies around high-redshift quasars, can we detect their Lyα emission lines without significant IGM attenuation? (2) How can we use galaxies near $z > 6$ quasars to constrain the Lyα escape fraction of EoR galaxies?

This Letter is organized as follows. Section 2 describes the NIRCam and NIRSpec observations used in this study. In Section 3, we describe how we measure the Lyα line properties of the targeted galaxies, and present evidence of less attenuated Lyα lines from galaxies near the luminous quasars. In Section 4, we evaluate the escape fraction of galaxies near quasars utilizing the high IGM transmission around quasars, and discuss the implications for reionization models. We draw conclusions in Section 5. Throughout this Letter, we adopt a flat ΛCDM cosmology with $H_0 = 70 \, \mathrm{km \, s^{-1}}$ and $\Omega_M = 0.3$, and use the AB magnitude system (J. B. Oke & J. E. Gunn 1983).

2. Data

2.1. NIRCam Observations

This work focuses on galaxies observed in two high-redshift quasar fields, namely around the quasars J0100+2802 ($z = 6.327$)
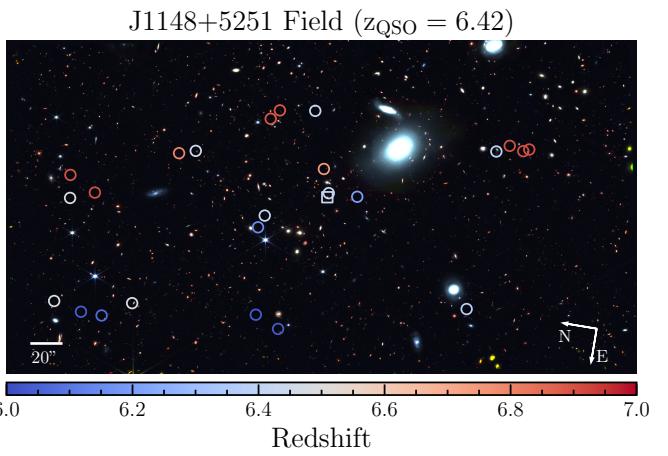
and J1148+5251 ($z = 6.42$). These quasar fields were observed as part of the Emission-line galaxies and Intergalactic Gas in the Epoch of Reionization (EIGER) program (GO-1243, PI: Lilly), which delivers NIRCam F115W, F200W, and F356W imaging and F356W grism spectroscopy. Figure 1 shows the NIRCam images of the two quasar fields. The images have sizes of $3' \times 6'$, which corresponds to $\approx 1 \times 2$ proper Mpc at the quasars' redshifts. We refer the reader to D. Kashino et al. (2023) and J. Matthee et al. (2023) for details on the data reduction of the EIGER observations. The typical 5σ depths of the F115W, F200W, and F356W imaging are 27.8, 28.3, and 28.1 mag, respectively. The sensitivity of the F356W grism spectra depends on the wavelength and the source positions, with the best sensitivity reaching $0.6 \times 10^{-18} \, \mathrm{erg \, s^{-1} \, cm^{-2}}$ at 3.8 μm.

Using the F356W grism spectra, J. Matthee et al. (2023) and D. Kashino et al. (2025) identified [O III] emitters in the two quasar fields and performed spectral energy distribution (SED) fitting for these galaxies. In this work, we use the [O III] redshifts as the systemic redshifts (z_{sys}) of galaxies. We also estimate the absolute magnitude at rest-frame 1500 Å (M_{UV}) of all the galaxies by fitting a power-law SED to the F115W and F200W magnitudes. These galaxy properties can be found in Table 1.

2.2. NIRSpec/MSA Spectroscopy

We obtain the NIRSpec/MSA G140M/F070LP spectroscopy for the two quasar fields as part of the Mapping Super-luminous Quasars' Extended Radiative Emission project (GO-3117 and GO-4713, PI: Eilers). The spectra cover wavelengths from $8000 \, \mathrm{Å} \lesssim \lambda_{\mathrm{obs}} \lesssim 13000 \, \mathrm{Å}$, with a wavelength-dependent spectral resolution of $R \approx 600$–1000. At the quasars' Lyα wavelengths ($\lambda_{\mathrm{obs}} \approx 9000 \, \mathrm{Å}$), the spectral resolution is $R \approx 600$. Each quasar field is covered by two MSA pointings, and we adopt the three-shutter dither pattern for the observations. The total on-source exposure time on each pointing is 7.7 hr.

The primary targets of the MSA observation are [O III] emitters at $z_{\mathrm{sys}} > 5.5$ in the quasar fields. In this study, we focus on galaxies at $z_{\mathrm{sys}} > 6$ and with $M_{\mathrm{UV}} < -19$, as the MSA observations are not sufficiently deep to detect the continuum of fainter sources. The circles in Figure 1 show the

location of the galaxies we analyze in this work, and the galaxy coordinates can be found in Table 1.

We reduce the spectra by running the Detector1Pipe-line using jwst[11] version 1.17.1 and CRDS jwst_1322. pmap to get the rate files, then using msaexp[12] version 0.9.5. dev8+ge2b237b (G. Brammer 2023) to extract the 2D spectra. As the final step, we use PypeIt (J. X. Prochaska et al. 2020)[13] version 1.17.1 to coadd the 2D spectra for individual objects and extract their 1D spectra.

Although not analyzed in this work, we also extract the spectra of $M_{\rm UV} > -19$ galaxies targeted by the MSA observation (36 galaxies in total). These spectra are available online at Zenodo: DOI: 10.5281/zenodo.17188912. Detailed analysis for galaxies will be presented in future studies.

3. Unattenuated Lyα Lines from Galaxies near Quasars

Luminous quasars at $z > 6$ are expected to produce large ionized bubbles around them, where the IGM has low opacity to Lyα photons. In this section, we test whether we can measure the Lyα lines from galaxies near quasars without significant IGM attenuation. We first fit the galaxy spectra to measure their Lyα fluxes, then compare the Lyα profiles and equivalent widths (EWs) of galaxies near quasars to galaxies outside the quasars' ionized bubbles.

3.1. Fitting the Lyα Lines

We fit the Lyα lines of galaxies targeted by the NIRSpec/MSA observation. We exclude five objects that have their Lyα lines falling in the detector gap, and three objects that are severely contaminated by nearby bright sources. For each remaining object, we fit the spectral window $1200\,{\rm \mathring{A}} < \lambda_{\rm rest} < 1500\,{\rm \mathring{A}}$, where $\lambda_{\rm rest} = \lambda_{\rm obs}/(1 + z_{\rm sys})$ is the rest-frame wavelength. We use a power-law continuum plus a Gaussian profile to model the spectral region around the Lyα emission, where the continuum flux at $\lambda_{\rm rest} < \lambda_{\rm Ly\alpha}$ is set to be zero. This model contains five free parameters, namely an amplitude (A) and a slope (β) of each galaxy's continuum, the Lyα redshift ($z_{\rm Ly\alpha}$), the Lyα flux ($F_{\rm Ly\alpha}$), and the line width ($\sigma_{\rm Ly\alpha}$). We run a nested sampling algorithm dynesty to determine the posterior probability distribution for each model parameter, where we adopt flat priors for all the parameters. We adopt the median of the posterior samples as fitting results, and determine their uncertainties from the 16th and 84th percentile. We test the impact of priors by running the fit with Gaussian priors, and find that the specific choice for priors has negligible impact on the fitting result.

Given the spectral resolution of the G140M grating, which is approximately $500\,{\rm km\,s^{-1}}$ at the Lyα wavelength, the Lyα lines are mostly unresolved or only marginally resolved. Therefore, we use a Gaussian profile to describe the Lyα line without modeling more complex line structures (such as asymmetries and outflows). This approach is sufficient for measuring the Lyα line fluxes and EWs, but does not allow us to identify any double-peak Lyα emitters (LAEs), as the peak separation is typically $\lesssim 500\,{\rm km\,s^{-1}}$ (e.g., A. Verhamme et al. 2018; R. P. Naidu et al. 2022).

Note that we aim to test whether galaxies near quasars show less attenuated Lyα lines compared to galaxies outside the quasars' ionized bubble. Therefore, we need to exclude possible active galactic nuclei (AGNs) from our sample, as AGNs may also produce their own ionized bubbles and show unattenuated Lyα lines. We identify possible AGNs by measuring the C IV line fluxes (e.g., K. Nakajima et al. 2018; A. Saxena et al. 2022). For each galaxy in our sample, we fit its spectrum at $1500\,{\rm \mathring{A}} < \lambda_{\rm rest} < 1600\,{\rm \mathring{A}}$ as a power-law continuum plus a Gaussian emission line. We find five galaxies with rest-frame C IV EW higher than $12\,{\rm \mathring{A}}$; according to K. Nakajima et al. (2018), these objects are likely AGNs, and we exclude them from the rest of this section. We present more information about these C IV emitters in the Appendix.

The final sample for this work consists of 50 galaxies at $6 < z < 7$ with $M_{\rm UV} < -19$, including 28 galaxies in the J0100 +2802 field and 22 galaxies in the J1148+5251 field. The median $M_{\rm UV}$ of this sample is -19.97. Of these, 14 galaxies have a Lyα line detection with $>3\sigma$ significance. Table 1 summarizes the properties of the galaxies in our sample.

We end this subsection by discussing the faint galaxies ($M_{\rm UV} < -19$) targeted by our MSA observation, which are not included in the final sample. We fit the Lyα lines for these galaxies, and 12 of them have Lyα line detections at $>3\sigma$ levels. The Lyα line fluxes and EWs (or the upper and lower limits of these quantities) for these $M_{\rm UV} < -19$ galaxies are available online at the GitHub repository[14] for the reader's reference.

3.2. The Lyα Profile of Galaxies near Quasars

We now investigate the Lyα line profiles for galaxies near the quasars. Due to the IGM's absorption, most $z > 6$ galaxies have no flux immediately blueward of their systemic Lyα wavelengths. In contrast, for galaxies residing within ionized bubbles generated by luminous quasars, the blue wing of their Lyα lines is expected to be visible due to the low IGM opacity. To investigate this effect, we stack the spectra of galaxies in our sample, as the spectra of individual galaxies do not have sufficient signal-to-noise ratio. Specifically, we consider three subsets of the galaxies:

1. $|z - z_{\rm Q}| < \frac{(1 + z_{\rm Q})\Delta v_{\rm max}}{c}$, where we take $\Delta v_{\rm max} = 2500\,{\rm km\,s^{-1}}$ in this work, and z_Q is the quasar's redshift. This sample is referred to as "galaxies near quasars";
2. $6 < z < z_{\rm Q} - \frac{(1 + z_{\rm Q})\Delta v_{\rm max}}{c}$, referred to as "foreground galaxies";
3. $z_{\rm Q} + \frac{(1 + z_{\rm Q})\Delta v_{\rm max}}{c} < z < 7$, referred to as "background galaxies."

We note here that all the targeted galaxies have transverse distances to the quasars of $r_\perp \lesssim 1$ proper Mpc. The expected sizes of the ionized bubble around $z > 6$ luminous quasars is $\gtrsim 1$ Mpc, given the typical quasar lifetimes ($\gtrsim 10^6$ yr; e.g., A.-C. Eilers et al. 2017; also see A.-C. Eilers et al. 2025). Therefore, we do not apply a cut on $r_\perp$ when selecting the "galaxies near quasars" sample.

For each subset, we select galaxies with at least 2σ detection for the Lyα flux. We subtract the best-fit continuum model (from Section 3.1) from the spectrum of each galaxy and shift the spectrum to the rest frame according to its systemic

---
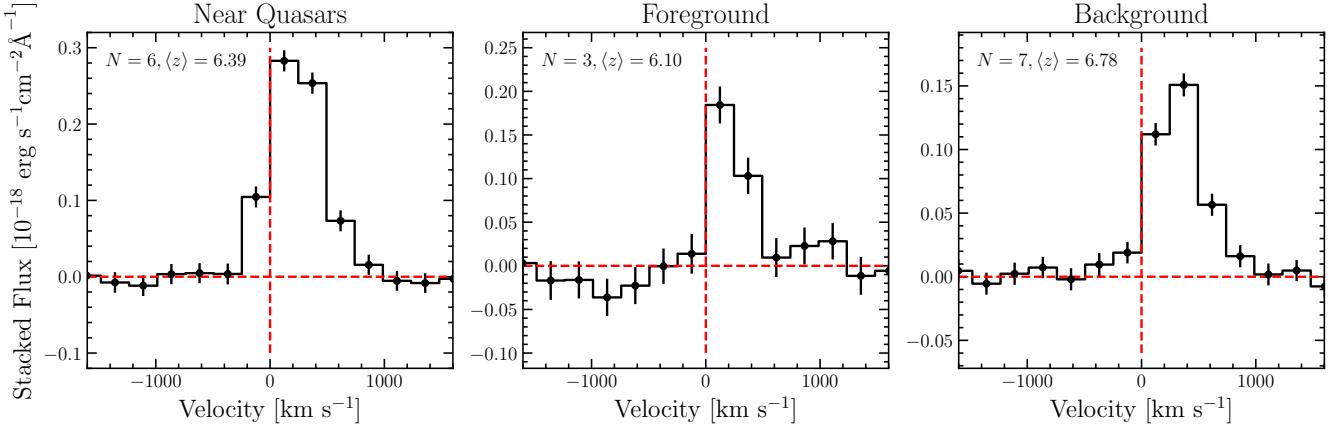
Figure 2. The stacked Lyα line profile for galaxies near quasars (left), foreground galaxies (middle), and background galaxies (right). The text in each panel marks the number of galaxies and the average redshift for the stacked spectra. The dashed lines mark the systemic Lyα wavelength and the level of zero flux. Galaxies near quasars show significant flux bluer than the systemic Lyα wavelength, indicating low IGM opacity around quasars. In contrast, the foreground and background galaxies do not have significant flux bluer than the Lyα wavelength.

Table 1
Properties of Galaxies in Our Sample

ID	R.A. (deg)	Decl. (deg)	z_{sys}	M_{UV} (mag)	$z_{Ly\alpha}$	$F_{Ly\alpha}$ (10^{-18} erg s^{-1} cm^{-2})	EW$_{Ly\alpha}^{rest}$ (Å)	$f_{esc}^{Ly\alpha}$
J1148_2637	177.112276	52.869027	6.037	−20.45	⋯	<2.76	<12.19	<0.034
J1148_3391	177.117208	52.902130	6.075	−20.07	⋯	<0.59	<2.51	<0.016
J1148_3461	177.109067	52.873590	6.039	−20.24	⋯	<0.70	<3.59	<0.081
J1148_3608	177.117109	52.906070	6.042	−19.19	$6.0449^{+0.0008}_{-0.0008}$	$3.10^{+0.55}_{-0.47}$	$34.34^{+10.88}_{-8.04}$	0.300 ± 0.251
J1148_3822	177.096543	52.834714	6.375	−19.97	⋯	<1.71	<90.55	<0.597
J1148_4246	177.111852	52.896855	6.485	−19.63	⋯	<2.50	<27.07	<0.273

(This table is available in its entirety in machine-readable form in the online article.)

redshift. We then regrid the spectra to a common wavelength grid and stack the spectra using inverse-variance weighting. The uncertainties of the stacked spectra are derived by propagating the errors of the individual objects' spectra.

Figure 2 presents the stacked spectra. The stacked spectra of galaxies near quasars show significant flux bluer than the systemic Lyα wavelength. In contrast, the stacked spectra for foreground and background galaxies do not have significant flux blueward of the systemic Lyα wavelength. This result supports the scenario where quasars enhance the Lyα transmission of their surrounding IGM, enabling the detection of Lyα blue wings for galaxies near quasars. Again, we note that the G140M grating does not have sufficient resolution to unveil the complex line structures (e.g., the double peaks) of the Lyα lines.

To further validate our result and ensure the comparison in Figure 2 is not dominated by individual objects, we bootstrap 100 times for the spectral stacking, and evaluate the mean and standard deviation of the bootstrapped stacked spectra. The bootstrapped spectra confirm our finding, i.e., the galaxies around quasars sample has strong a flux bluer than the Lyα wavelength, while the other two samples have zero flux bluer than Lyα.

3.3. The Lyα Equivalent Width Distribution

We then evaluate the rest-frame Lyα EW (EW$_{Ly\alpha}^{rest}$) of the targeted galaxies. If the IGM around quasars has low opacity to Lyα photons, galaxies near high-redshift quasars should

show higher EW$_{Ly\alpha}^{rest}$ compared to other galaxies at similar redshifts.

The top and middle panels of Figure 3 show the Lyα luminosity and EW of individual galaxies in our sample. The red dashed line marks the quasars' redshifts, and the shaded region represents the region around the quasars (i.e., $\Delta v < 2500$ km s^{-1}). Among the 15 galaxies near quasars, six (40%) of them have Lyα lines detected at higher than 3σ significance. In contrast, this fraction is only $8/35 = 22.9\%$ for foreground and background galaxies. The fractions of galaxies with EW$_{Ly\alpha}^{rest} > 10$ Å are $5/15 = 33.3\%$ and $7/35 = 20.0\%$ for galaxies near quasars and foreground/background galaxies, respectively. This comparison already hints that galaxies around quasars have less attenuated Lyα emissions, due to the low IGM opacity in the quasar's proximity zone.

To further quantify the difference in Lyα emissions between galaxies inside and outside the quasars' ionized bubbles, we estimate the distribution of EW$_{Ly\alpha}^{rest}$ for galaxies in our sample. We follow the Bayesian analysis in M. Tang et al. (2024b; also see M. A. Schenker et al. 2014; R. Endsley et al. 2021; K. N. K. Boyett et al. 2022; Z. Chen et al. 2024). Specifically, we assume a lognormal distribution for EW$_{Ly\alpha}^{rest}$:

$$p(x|\mu, \sigma) = \frac{A}{\sqrt{2\pi}\,\sigma x} \times \exp\left[-\frac{(\ln x - \mu)^2}{2\sigma^2}\right], \quad (1)$$

where x is the random variable (EW$_{Ly\alpha}^{rest}$ in this case), μ and σ are the mean and standard deviation of the lognormal
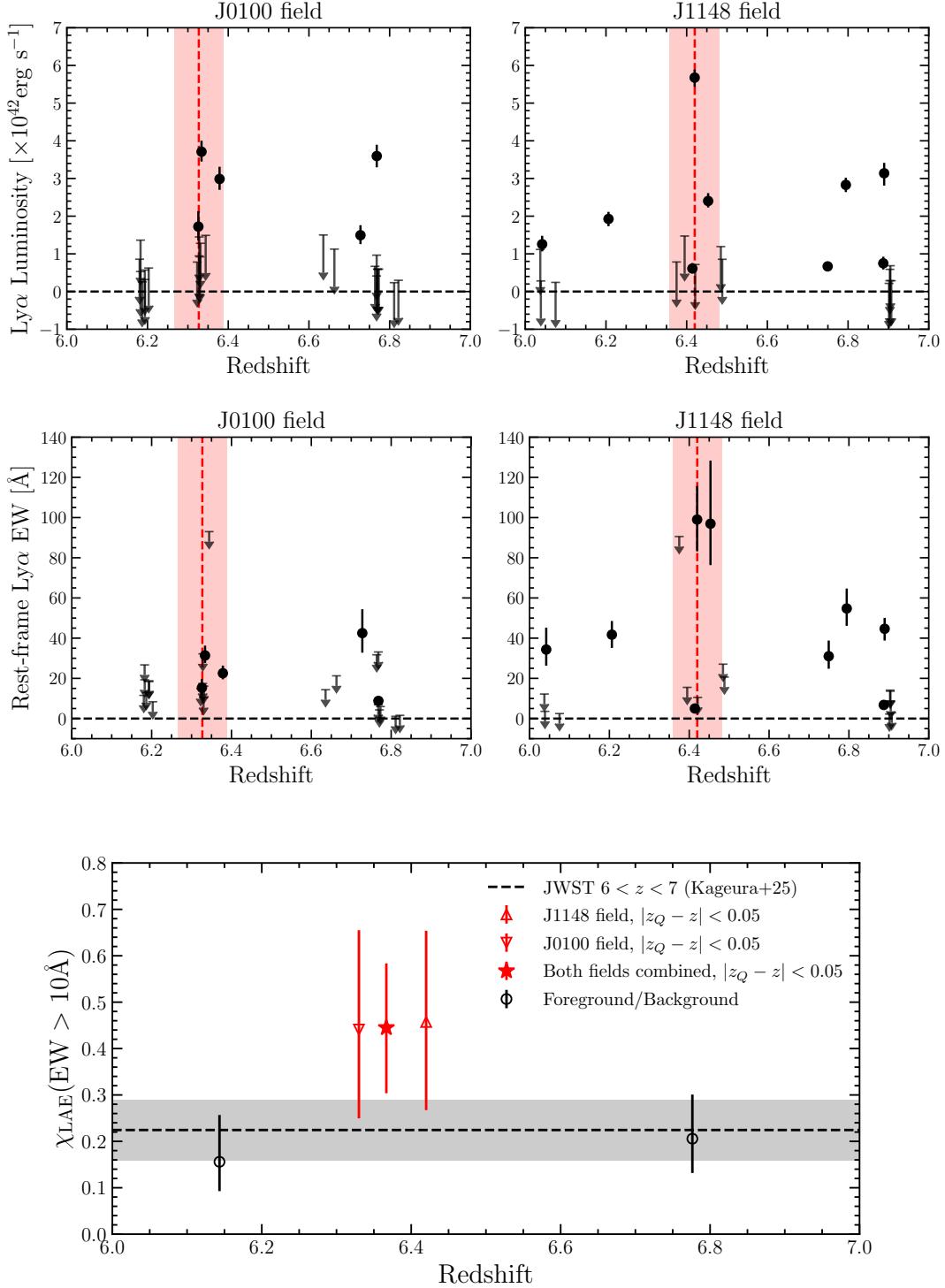
Figure 3. Top panels: redshift and Lyα luminosity distribution of galaxies in the J0100 field and the J1148 field, in the left and right panel, respectively. The red shaded region marks the quasar's vicinity $|\Delta v| < 2500$ km s^{-1}. Middle panels: similar to the top panel, but for the redshift and Lyα EW distribution. Bottom: the fraction of galaxies with EW$_{Ly\alpha}^{rest} > 10$ Å. This fraction is estimated by fitting the galaxy EW$_{Ly\alpha}^{rest}$ with a lognormal distribution (see text for details). We also include the NIRSpec-observed galaxies at $6 < z < 7$ from Y. Kageura et al. (2025) for comparison. In both quasar fields, galaxies in the quasar's vicinity show higher LAE fractions than foreground and background galaxies and the general galaxy population. This comparison indicates that the IGM around luminous quasars has high transmission to Lyα photons.

distribution, and A is the normalization. We derive the posterior distribution of (μ, σ) according to Bayes' theorem:

$$p(\mu, \sigma|\text{obs}) \propto p(\text{obs}|\mu, \sigma)p(\mu, \sigma), \qquad (2)$$

where $p(\mu, \sigma)$ is the prior, and we adopt flat priors for μ and σ. $p(\text{obs}|\mu, \sigma)$ is the probability of getting the observed EW$_{Ly\alpha}^{rest}$

for the galaxies. Specifically,

$$p(\text{obs}|\mu, \sigma) = \prod_i p(\text{obs}, i|\mu, \sigma)$$
$$= \prod_i \int_0^{+\infty} p(x)_{\text{obs},i} \cdot p(x|\mu, \sigma) \, dx, \qquad (3)$$

Table 2
The EW$_{\rm Ly\alpha}^{\rm rest}$ Distribution of Galaxies

Sample	$\langle z \rangle$	Detection Fraction[a]	μ(EW$_{\rm Ly\alpha}^{\rm rest}$) (Å)	σ(EW$_{\rm Ly\alpha}^{\rm rest}$) (Å)	$\chi_{\rm LAE}$ (EW > 10 Å)	$\chi_{\rm LAE}$ (EW > 25 Å)
Galaxies near quasars	6.37	6/15	$2.07^{+0.53}_{-0.89}$	$1.70^{+0.89}_{-0.51}$	$0.45^{+0.14}_{-0.14}$	$0.24^{+0.11}_{-0.08}$
Foreground galaxies	6.14	2/12	$-0.89^{+1.63}_{-1.40}$	$3.14^{+1.10}_{-1.08}$	$0.16^{+0.10}_{-0.06}$	$0.09^{+0.07}_{-0.05}$
Background galaxies	6.71	6/23	$0.03^{+0.91}_{-1.23}$	$2.86^{+1.05}_{-0.78}$	$0.21^{+0.10}_{-0.07}$	$0.12^{+0.08}_{-0.05}$
Foreground + background	6.53	8/35	$0.00^{+0.78}_{-1.20}$	$2.61^{+0.99}_{-0.68}$	$0.19^{+0.06}_{-0.06}$	$0.10^{+0.05}_{-0.04}$
Y. Kageura et al. (2025)[b]	6.42	⋯	$0.76^{+0.63}_{-0.92}$	$1.96^{+0.76}_{-0.46}$	$0.22^{+0.07}_{-0.06}$	$0.11^{+0.04}_{-0.04}$

Notes. All samples are selected to have $M_{\rm UV} < -19$.
[a] The fraction of galaxies with at least 3σ detection of their Lyα line.
[b] Galaxies observed by NIRSpec at $6 < z < 7$, as compiled by Y. Kageura et al. (2025).

where i goes through all galaxies in the sample, and $p(x)_{{\rm obs},i}$ is the posterior distribution of the galaxies' EW$_{\rm Ly\alpha}^{\rm rest}$. For galaxies with $>3\sigma$ Lyα line detection, we assume a Gaussian error for the detection, i.e.,

$$p(x)_{{\rm obs},i} = \frac{1}{\sqrt{2\pi}\,\sigma_{{\rm obs},i}} \cdot \exp\left[-\frac{(x - x_{{\rm obs},i})^2}{2\sigma_{{\rm obs},i}^2}\right]. \quad (4)$$

For upper limits, we have

$$p({\rm obs},\,i|\mu,\,\sigma) = p(x < x_{3\sigma,i}^{\rm lim}|\mu,\,\sigma). \quad (5)$$

We run Markov Chain Monte Carlo to sample the posterior of $(\mu,\,\sigma)$.

Using this method, we model the EW$_{\rm Ly\alpha}^{\rm rest}$ distributions for galaxies near quasars, foreground galaxies, and background galaxies. For comparison, we also fit the distributions for NIRSpec-observed $6 < z < 7$ galaxies compiled by Y. Kageura et al. (2025). When fitting the galaxies from Y. Kageura et al. (2025), we apply a cut of $M_{\rm UV} < -19$ to match the absolute magnitude of our sample.

Table 2 lists the best-fit parameters for these galaxy subsets. Using the posterior of $(\mu,\,\sigma)$, we also compute the LAE fractions (defined as galaxies with EW$_{\rm Ly\alpha}^{\rm rest} > 10$ Å) for the subsets of galaxies, which are shown in the bottom panel of Figure 3. The foreground and background galaxy samples have LAE fractions close to the $6 < z < 7$ galaxy sample from Y. Kageura et al. (2025). In contrast, in both quasar fields, galaxies near quasars show higher LAE fractions. This comparison again indicates that galaxies near quasars have less attenuated Lyα lines compared to other $z > 6$ galaxies, due to the low IGM opacity around quasars. Note that the UV-slope and UV-magnitude distributions of galaxies near quasars are very similar to those of foreground and background galaxies; therefore, the difference in EW$_{\rm Ly\alpha}^{\rm rest}$ can only be attributed to the difference in IGM opacity, i.e., the influence of the quasars' ionizing radiation fields.

We notice that galaxies near quasars have LAE fractions μ(EW$_{\rm Ly\alpha}^{\rm rest}$) similar to $z \sim 5$ galaxies measured by M. Tang et al. (2024b). Our result indicates that the unattenuated Lyα line EW of $M_{\rm UV} < -19$ galaxies has little evolution from $z \sim 6.4$ to $z \sim 5$.

We also note that including C IV emitters into the EW$_{\rm Ly\alpha}^{\rm rest}$ distribution has a negligible impact on the derived LAE fractions. By including the C IV emitters, the EW$_{\rm Ly\alpha}^{\rm rest} > 10$ Å fraction of galaxies near quasars changes to $\chi_{\rm LAE}$(EW > 10 Å) =

$0.44^{+0.15}_{-0.14}$, and that of foreground + background galaxies changes to $\chi_{\rm LAE}$(EW > 10 Å)$=0.24^{+0.07}_{-0.06}$.

3.3.1. How Does the Quasars' Radiation Affect Galaxy Properties?

The analysis above assumes that the quasars' radiation fields do not significantly affect the intrinsic Lyα properties of their surrounding galaxies. If the quasars' radiation enhances the star formation and/or the Lyα escape fraction of nearby galaxies, we expect to see a high LAE fraction for galaxies near quasars even without a low IGM opacity. In this subsection, we discuss the possible impact of the quasars' radiation field on galaxy properties.

We first evaluate the strength of a quasar's radiation field at the position of its surrounding galaxies. The brighter quasar in our sample, J0100+2802, has $M_{\rm UV} = 29$ (C. Mazzucchelli et al. 2023). The faintest galaxy in our sample has $M_{\rm UV} < -19$, i.e., 10^4 times fainter than the quasar. The transverse distances from the galaxies to the quasars are $r_\perp \gtrsim 0.5$ Mpc. Assuming a typical galaxy size of 1 kpc, we estimate the quasars' radiation fields should be $\lesssim 4\%$ of the galaxies' own radiation. This comparison suggests that quasars should have little impact on the surrounding galaxies' star formation. This argument is strengthened by the short lifetimes of quasars ($\lesssim 1$ Myr; e.g., I. S. Khrykin et al. 2021; A.-C. Eilers et al. 2025), given that the Lyα line traces the star formation in the past several Myr (e.g., D. Sobral & J. Matthee 2019).

Another way to investigate the potential impact of quasars on their surrounding galaxies is by artificially adding IGM attenuation to the galaxies near quasars. The IGM at $z \sim 6.3$–6.4 primarily absorbs the blue wings of Lyα lines without causing significant damping absorption for the red wings; therefore, we expect that the increased transmission in the vicinity of quasars enhances the Lyα flux of galaxies near quasars by no more than a factor of 2. If we reduce the observed Lyα flux of galaxies near quasars by a factor of 2 and still see an enhancement in Lyα emission, it will indicate that quasar radiation boosts the Lyα emission in nearby galaxies.

Following this argument, we divide the Lyα fluxes of the galaxies near quasars by 2 and reperform the analysis. The derived LAE fraction for galaxies near quasars is $0.28^{+0.11}_{-0.09}$, close to the $6 < z < 7$ galaxy sample. Figure 3 also implies that, with their Lyα fluxes divided by 2, galaxies near quasars will be indistinguishable from foreground and background galaxies. In other words, our data set shows no clear evidence that quasar radiation significantly boosts the intrinsic Lyα emission of galaxies near quasars.

Finally, we note that our data set is not able to fully distinguish the influence of IGM opacity and intrinsic Lyα line properties for galaxies near quasars. Future high-resolution spectroscopy for these galaxies will provide resolved Lyα profiles of these galaxies, which will enable modeling of the IGM transmission profile around the quasars and break the degeneracy discussed above.

4. Implication for the Escape Fraction of Reionization-epoch Galaxies

The enhanced EW$_{\rm Ly\alpha}^{\rm rest}$ and the detection of the Lyα blue wing for galaxies near quasars indicate that we can detect the Lyα emission line from these galaxies without significant IGM attenuation. These galaxies provide a rare opportunity to directly constrain the Lyα emission lines properties of $z > 6$ galaxies, which is usually impossible due to the high IGM neutral fraction ($x_{\rm HI} \gtrsim 0.1$; e.g., X. Jin et al. 2023; D. Ďurovčíková et al. 2024). As an example, in this section, we use galaxies near quasars in our sample to put direct constraints on the Lyα escape fraction ($f_{\rm esc}^{\rm Ly\alpha}$) of $z > 6$ galaxies.

To evaluate $f_{\rm esc}^{\rm Ly\alpha}$, for each galaxy, we adopt the Hβ flux from the [O III] emitter catalog presented in J. Matthee et al. (2023) and D. Kashino et al. (2025). We note that one galaxy does not have Hβ measurement and is excluded from the escape fraction analysis. We obtain the dust attenuation (A_V) from the catalog and correct the Hβ fluxes for dust attenuation. The median attenuation of the sample is 0.22 mag. We also estimate the continuum flux at $\lambda_{\rm rest} = 1215.67$ Å (denoted by $F_{\rm cont}^{1215.67\,\text{Å}}$) by fitting its F115W and F200W magnitudes using a power-law SED. We then compute the escape fraction as

$$f_{\rm esc}^{\rm Ly\alpha} = \frac{{\rm EW}_{\rm Ly\alpha}^{\rm rest} \times F_{\rm cont}^{1215.67\,\text{Å}}}{25 \times F_{\rm H\beta}}, \tag{6}$$

where EW$_{\rm Ly\alpha}^{\rm rest}$ comes from fitting the MSA spectra, and the coefficient 25 corresponds to case B recombination with temperature $T = 10^4$ K (e.g., M. Tang et al. 2024a; Y. Kageura et al. 2025). This approach avoids possible impacts due to the slitloss of the MSA slitlets.

With the $f_{\rm esc}^{\rm Ly\alpha}$ of individual galaxies, we compute the distribution of $f_{\rm esc}^{\rm Ly\alpha}$ following the same method we use for evaluating the EW$_{\rm Ly\alpha}^{\rm rest}$ distribution as described in Section 3.3. Specifically, we assume a lognormal distribution for $f_{\rm esc}^{\rm Ly\alpha}$, and use Equations (1)–(5) to evaluate the posterior of (μ, σ) for the distribution. For galaxies near quasars, we get $\mu = -2.78_{-1.19}^{+1.48}$ and $\sigma = 3.41_{-1.39}^{+1.06}$. These numbers indicate an average escape fraction of $f_{\rm esc}^{\rm Ly\alpha} = 0.14 \pm 0.04$, consistent with the measurements for $z \lesssim 5$ galaxies (e.g., X. Lin et al. 2024).

The LyC escape fraction is positively correlated with the Lyα escape fraction, and most galaxies have $f_{\rm esc}^{\rm LyC} < f_{\rm esc}^{\rm Ly\alpha}$ (e.g., M. Dijkstra et al. 2016; A. Verhamme et al. 2017). We estimate the average LyC escape fraction for galaxies near quasars using the relation in R. Begley et al. (2024), who suggested that $f_{\rm esc}^{\rm LyC} = 0.15 \times f_{\rm esc}^{\rm Ly\alpha}$. This relation gives $f_{\rm esc}^{\rm LyC} \approx 0.02 \pm 0.01$. We note that the $f_{\rm esc}^{\rm LyC} - f_{\rm esc}^{\rm Ly\alpha}$ relation has large scatter and might depend on the properties of galaxies; therefore, we take $f_{\rm esc}^{\rm LyC} < f_{\rm esc}^{\rm Ly\alpha} \approx 0.14$ as a conservative upper limit. Due to the small sample size (15 galaxies in total, where 6 galaxies have Lyα detections), we are not able to further explore the correlation between $f_{\rm esc}^{\rm Ly\alpha}$

and other galaxy properties (like $M_{\rm UV}$ and UV slope; e.g., L. Anderson et al. 2017; J. Chisholm et al. 2022).

Our analysis demonstrates the unique power of high-redshift quasar fields in measuring the escape fraction of EoR galaxies. The estimated $f_{\rm esc}^{\rm LyC}$ disfavors the "high escape fraction" scenario with $f_{\rm esc}^{\rm LyC} \gtrsim 0.2$ (e.g., R. P. Naidu et al. 2020), at least for galaxies with $M_{\rm UV} < -19$ at $z \sim 6.4$. Given the UV luminosity functions of $z > 6$ galaxies (e.g., R. J. Bouwens et al. 2022), a low escape fraction of $f_{\rm esc}^{\rm LyC} \approx 2\%$ indicates that luminous galaxies (e.g., those with $M_{\rm UV} < -18$) cannot make a major contribution to the ionizing photon production. In a recent study, C. Simmonds et al. (2024) measured the ionizing photon production efficiency ($\xi_{\rm ion}$) for $3 < z < 9$ galaxies using NIRCam imaging. With the $\xi_{\rm ion}(M_{\rm UV}, z)$ they presented, we only need a low escape fraction $f_{\rm esc}^{\rm LyC} \lesssim 0.05$ to reionize the Universe. This picture is consistent with our measurement. The estimated $f_{\rm esc}^{\rm LyC}$ is also consistent with the finding of C. Papovich et al. (2025), who performed stellar population and nebular emission modeling for $4.5 < z < 9.0$ observed using JWST imaging and prism spectroscopy and found an average escape fraction of $f_{\rm esc}^{\rm LyC} = 0.03 \pm 0.01$.

4.1. Systematic Uncertainties

In order to measure the $f_{\rm esc}^{\rm Ly\alpha}$ for galaxies near quasars, we need to assume that these galaxies have negligible IGM attenuation for their Lyα lines. Here we discuss the systemic uncertainties introduced by this assumption. The Lyα blue wing in the stacked spectra (Figure 2) indicates that the IGM opacity around the quasars is similar to that of $z \sim 5$ IGM (e.g., M. J. Hayes et al. 2021). This similarity is further supported by the recent transverse proximity effect measurement for J0100 +2802 (Eilers et al. 2025, submitted). In short, Eilers et al. (2025, submitted) measured the transmission flux for background galaxies ($z > z_Q + 0.1$) and found a Lyα transmission of $\mathcal{T} \gtrsim 0.5$ for the IGM near the quasar. In comparison, IGM at $z \lesssim 5$ has transmission of $\mathcal{T} \gtrsim 0.1$ (e.g., R. Thomas et al. 2021; R. A. Meyer et al. 2025). We also notice that the IGM attenuation for Lyα line fluxes is $\lesssim 10\%$ at $z \lesssim 5$ (e.g., M. J. Hayes et al. 2021; J. Matthee et al. 2022). We thus expect the uncertainty introduced by our assumption to be smaller than 10%. This uncertainty does not influence our main result, i.e., the average Lyα escape fraction is about 0.14.

Another major uncertainty is from the limited sample size, as the "galaxies near quasars" sample only contains 15 galaxies. Future NIRSpec/MSA observations for more high-redshift quasars will reduce the survey variance and provide tighter constraints on the escape fraction of $z > 6$ galaxies.

5. Conclusion

We present JWST NIRSpec/MSA observations for galaxies in two high-redshift quasar fields, namely J0100 +2802 ($z = 6.327$) and J1148+5251 ($z = 6.42$). We analyze 50 galaxies at $6 < z < 7$ with $M_{\rm UV} < -19$, among which 15 are located near the quasars (with $\Delta v < 2500$ km s^{-1}). We measure the Lyα fluxes, profiles, and rest-frame EWs of these galaxies. Leveraging the low IGM opacity around quasars, we are able to measure the Lyα lines from galaxies near quasars without significant IGM attenuation. This allows us to put direct constraints on the Lyα escape fraction of $z > 6$ galaxies. Our main findings include the following.

1. The stacked Lyα spectrum for galaxies near quasars clearly shows a significant emission bluer than the systemic Lyα wavelength, while foreground and background galaxies show no significant emission bluer than the systemic Lyα wavelength in their stacked spectra. This result indicates that the Lyα lines from galaxies near high-redshift quasars are less attenuated compared to other galaxies at similar redshifts.

2. The LAE fraction of galaxies near quasars is $\chi_{\rm LAE}({\rm EW} > 10\,{\rm Å}) = 0.45^{+0.14}_{-0.14}$, higher than that of foreground and background galaxies ($0.19^{+0.06}_{-0.06}$). This result confirms that galaxies near quasars have less attenuated Lyα lines. The ${\rm EW}^{\rm rest}_{\rm Ly\alpha}$ distribution of galaxies near quasars is similar to $z \sim 5$ galaxies.

3. We estimate a median Lyα escape fraction of $f^{\rm Ly\alpha}_{\rm esc}=0.14 \pm 0.04$ for galaxies near quasars. Adopting the scaling relation of $f^{\rm LyC}_{\rm esc} = 0.15 \times f^{\rm Ly\alpha}_{\rm esc}$ from R. Begley et al. (2024), we estimate $f^{\rm LyC}_{\rm esc} = 0.02 \pm 0.01$ for galaxies near quasars. This result favors the low escape fraction scenario ($f^{\rm LyC}_{\rm esc} \lesssim 0.1$) for $z > 6$ galaxies.

The ionized bubbles surrounding luminous quasars serve as unique laboratories for studying galaxy evolution and reionization in the early Universe. High-resolution spectroscopy with NIRSpec's high-resolution grating or future extremely large telescopes will be able to resolve the Lyα line profiles of galaxies near high-redshift quasars (e.g., R. P. Naidu et al. 2022). Such observations will enable key measurements for EoR galaxies, such as outflow properties and interstellar medium conditions. These experiments will offer valuable insights into the physical properties of EoR galaxies.

The JWST data used in this Letter can be found in MAST: DOI: 10.17909/wm0b-5n06. All the code and data used in this work will be available online at GitHub: https://github.com/cosmicdawn-mit/MASQUERADE_LAE with a copy deposited to Zenodo: DOI: 10.5281/zenodo.17254903.

Acknowledgments

Appendix
C IV Emitters in Our Sample

In addition to the 50 galaxies in the main sample, we also identified five C IV emitters with ${\rm EW}_0$ (C iv) > 12 Å. These galaxies are possible AGNs. Three C IV emitters show Lyα emissions at $>3\sigma$ levels, two of which have ${\rm EW}^{\rm rest}_{\rm Ly\alpha} > 100$ Å. We highlight object J0100_10287 at $z = 6.77$, which has ${\rm EW}^{\rm rest}_{\rm Ly\alpha} = 152^{+60}_{-30}$ Å and is the strongest LAE in the MASQUERADE sample with $M_{\rm UV} < -19$. The properties of the C IV emitters are also included in Table 1.

Following the method in Section 3.2, we produce the stacked Lyα profile for the C IV emitters at the quasars' foreground and background. Although these galaxies are outside the quasars' ionized bubbles, the stacked Lyα spectrum shows a significant Lyα blue wing (Figure 4). This result indicates that these C IV emitters can produce their own ionized bubbles. Our finding is consistent with previous studies that suggest C IV emitters might be strong Lyα leakers (e.g., R. P. Naidu et al. 2022; D. Schaerer et al. 2022; S. Mascia et al. 2023).

We also note that only one C IV emitter is located in the ionized bubbles around quasars. Including this object in the "galaxies near quasars" sample has a negligible impact on the estimated ${\rm EW}^{\rm rest}_{\rm Ly\alpha}$ and $f^{\rm Ly\alpha}_{\rm esc}$ distributions.
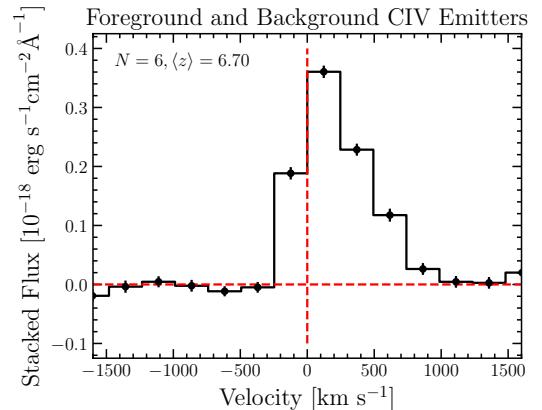
Figure 4. The stacked Lyα line for C IV emitters at the quasars' foreground and background, showing significant flux bluer than the systemic Lyα wavelength. This result indicates that C IV emitters can produce their own ionized bubbles.

ORCID iDs

Minghao Yue ⬥ https://orcid.org/0000-0002-5367-8021
Anna-Christina Eilers ⬥ https://orcid.org/0000-0003-2895-6218
Jorryt Matthee ⬥ https://orcid.org/0000-0003-2871-127X
Rohan P. Naidu ⬥ https://orcid.org/0000-0003-3997-5705
Rongmon Bordoloi ⬥ https://orcid.org/0000-0002-3120-7173
Frederick B. Davies ⬥ https://orcid.org/0000-0003-0821-3644
Joseph F. Hennawi ⬥ https://orcid.org/0000-0002-7054-4332
Daichi Kashino ⬥ https://orcid.org/0000-0001-9044-1747
Ruari Mackenzie ⬥ https://orcid.org/0000-0003-0417-385X
Robert A. Simcoe ⬥ https://orcid.org/0000-0003-3769-9559

References

Anderson, L., Governato, F., Karcher, M., Quinn, T., & Wadsley, J. 2017, MNRAS, 468, 4077
Ashton, G., Hübner, M., Lasky, P. D., et al. 2019, ApJS, 241, 27
Astropy Collaboration, Price-Whelan, A. M., Lim, P. L., et al. 2022, ApJ, 935, 167
Astropy Collaboration, Price-Whelan, A. M., Sipőcz, B. M., et al. 2018, AJ, 156, 123
Astropy Collaboration, Robitaille, T. P., Tollerud, E. J., et al. 2013, A&A, 558, A33
Atek, H., Labbé, I., Furtak, L. J., et al. 2024, Natur, 626, 975
Begley, R., Cullen, F., McLure, R. J., et al. 2024, MNRAS, 527, 4040
Bosman, S. E. I., Davies, F. B., Becker, G. D., et al. 2022, MNRAS, 514, 55
Bosman, S. E. I., Kakiichi, K., Meyer, R. A., et al. 2020, ApJ, 896, 49
Bouwens, R. J., Illingworth, G., Ellis, R. S., Oesch, P., & Stefanon, M. 2022, ApJ, 940, 55
Bouwens, R. J., Illingworth, G. D., Oesch, P. A., et al. 2012, ApJL, 752, L5
Boyett, K. N. K., Stark, D. P., Bunker, A. J., Tang, M., & Maseda, M. V. 2022, MNRAS, 513, 4451
Brammer, G. 2023, msaexp: NIRSpec Analyis Tools, v0.6.17, Zenodo, doi:10.5281/zenodo.8319596
Chen, Z., Stark, D. P., Mason, C., et al. 2024, MNRAS, 528, 7052
Chen, Z., Stark, D. P., Mason, C. A., et al. 2025, arXiv:2505.24080
Chisholm, J., Saldana-Lopez, A., Flury, S., et al. 2022, MNRAS, 517, 5104
Davies, F. B. 2020, MNRAS, 494, 2937
Dijkstra, M., Gronke, M., & Venkatesan, A. 2016, ApJ, 828, 71
Ďurovčíková, D., Eilers, A.-C., Chen, H., et al. 2024, ApJ, 969, 162
Eilers, A.-C., Davies, F. B., Hennawi, J. F., et al. 2017, ApJ, 840, 24
Eilers, A.-C., Yue, M., Matthee, J., et al. 2025, ApJL, 991, L40
Endsley, R., Stark, D. P., Charlot, S., et al. 2021, MNRAS, 502, 6044
Fan, X., Strauss, M. A., Becker, R. H., et al. 2006, AJ, 132, 117
Finkelstein, S. L., D'Aloisio, A., Paardekooper, J.-P., et al. 2019, ApJ, 879, 36
Hayes, M. J., Runnholm, A., Gronke, M., & Scarlata, C. 2021, ApJ, 908, 36
Izotov, Y. I., Chisholm, J., Worseck, G., et al. 2022, MNRAS, 515, 2864
Izotov, Y. I., Worseck, G., Schaerer, D., et al. 2018, MNRAS, 478, 4851

Jaskot, A. E., Silveyra, A. C., Plantinga, A., et al. 2024, ApJ, 973, 111
Jin, X., Yang, J., Fan, X., et al. 2023, ApJ, 942, 59
Kageura, Y., Ouchi, M., Nakane, M., et al. 2025, ApJS, 278, 33
Kashino, D., Lilly, S. J., Matthee, J., et al. 2023, ApJ, 950, 66
Kashino, D., Lilly, S. J., Matthee, J., et al. 2025, arXiv:2506.03121
Khrykin, I. S., Hennawi, J. F., Worseck, G., & Davies, F. B. 2021, MNRAS, 505, 649
Lin, X., Cai, Z., Wu, Y., et al. 2024, ApJS, 272, 33
Lu, T.-Y., Mason, C. A., Mesinger, A., et al. 2025, A&A, 697, A69
Ma, X., Hopkins, P. F., Kasen, D., et al. 2016, MNRAS, 459, 3614
Ma, X., Kasen, D., Hopkins, P. F., et al. 2015, MNRAS, 453, 960
Mascia, S., Pentericci, L., Calabrò, A., et al. 2023, A&A, 672, A155
Mason, C. A., Fontana, A., Treu, T., et al. 2019, MNRAS, 485, 3947
Mason, C. A., Treu, T., Dijkstra, M., et al. 2018, ApJ, 856, 2
Matthee, J., Mackenzie, R., Simcoe, R. A., et al. 2023, ApJ, 950, 67
Matthee, J., Naidu, R. P., Pezzulli, G., et al. 2022, MNRAS, 512, 5960
Matthee, J., Sobral, D., Gronke, M., et al. 2018, A&A, 619, A136
Mazzucchelli, C., Bischetti, M., D'Odorico, V., et al. 2023, A&A, 676, A71
Meyer, R. A., Roberts-Borsani, G., Oesch, P., & Ellis, R. S. 2025, MNRAS, 542, 1952
Naidu, R. P., Forrest, B., Oesch, P. A., Tran, K.-V. H., & Holden, B. P. 2018, MNRAS, 478, 791
Naidu, R. P., Matthee, J., Oesch, P. A., et al. 2022, MNRAS, 510, 4582
Naidu, R. P., Tacchella, S., Mason, C. A., et al. 2020, ApJ, 892, 109
Nakajima, K., Schaerer, D., Le Fèvre, O., et al. 2018, A&A, 612, A94
Nikolić, I., Mesinger, A., Mason, C. A., et al. 2025, A&A, 699, A323
Oke, J. B., & Gunn, J. E. 1983, ApJ, 266, 713
Papovich, C., Cole, J. W., Hu, W., et al. 2025, arXiv:2505.08870
Planck Collaboration, Aghanim, N., Akrami, Y., et al. 2020, A&A, 641, A6
Prochaska, J. X., Hennawi, J. F., Westfall, K. B., et al. 2020, JOSS, 5, 2308
Protušová, K., Bosman, S. E. I., Wang, F., et al. 2024, A&A, 700, A218
Robertson, B. E. 2022, ARA&A, 60, 121
Rosdahl, J., Blaizot, J., Katz, H., et al. 2022, MNRAS, 515, 2386
Saxena, A., Cryer, E., Ellis, R. S., et al. 2022, MNRAS, 517, 1098
Schaerer, D., Izotov, Y. I., Worseck, G., et al. 2022, A&A, 658, L11
Schenker, M. A., Ellis, R. S., Konidaris, N. P., & Stark, D. P. 2014, ApJ, 795, 20
Sharma, M., Theuns, T., Frenk, C., et al. 2016, MNRAS, 458, L94
Simmonds, C., Tacchella, S., Hainline, K., et al. 2024, MNRAS, 535, 2998
Sobral, D., & Matthee, J. 2019, A&A, 623, A157
Steidel, C. C., Bogosavljević, M., Shapley, A. E., et al. 2018, ApJ, 869, 123
Tang, M., Stark, D. P., Ellis, R. S., et al. 2024b, MNRAS, 531, 2701
Tang, M., Stark, D. P., Topping, M. W., Mason, C., & Ellis, R. S. 2024a, ApJ, 975, 208
Thomas, R., Pentericci, L., Le Fèvre, O., et al. 2021, A&A, 650, A63
Torralba, A., Matthee, J., Naidu, R. P., et al. 2024, A&A, 689, A44
Umeda, H., Ouchi, M., Kageura, Y., et al. 2025, arXiv:2504.04683
Verhamme, A., Garel, T., Ventou, E., et al. 2018, MNRAS, 478, L60
Verhamme, A., Orlitová, I., Schaerer, D., et al. 2017, A&A, 597, A13
Whitler, L., Stark, D. P., Endsley, R., et al. 2024, MNRAS, 529, 855
Wold, I. G. B., Malhotra, S., Rhoads, J., et al. 2022, ApJ, 927, 36
Yang, J., Wang, F., Fan, X., et al. 2020, ApJ, 904, 26